Journal of
Marine Science and Engineering

MDPI

Article

Cold Intermediate Water Formation in the Black Sea Triggered by March 2022 Cold Intrusions

Tülay Çokacar

Institute of Marine Sciences and Management, İstanbul University, İstanbul 34134, Türkiye; tulay.cokacar@istanbul.edu.tr

Abstract: In mid-March 2022, a Siberian High brought intense cold air masses, leading to severe weather conditions across southern Europe, including the Black Sea region. This study investigates the spatial and temporal evolution of cold intermediate water (CIW) masses in the Black Sea, with a particular focus on the successive anomalously cold episodes that occurred in March 2022. The research underscores the significance of the northwestern continental slope and cyclonic gyres, especially as the only cold-water mass observations during the warm winters of 2020 and 2021 were concentrated in these areas. Following two warm winters, the cold episodes of March 2022 revealed notable convection and simultaneous cooling, particularly in the cyclonic interior and the Rim Current periphery, excluding the northeastern periphery. Subsequently, cold waters spreading isopycnally throughout the summer months were transported laterally and reached these regions. Argo float measurements provided clear evidence of widespread replenishment of the CIW, indicating that it is not confined to specific areas. The study also highlights regional variability in the characteristics of CIW formation, which is influenced by local dynamics and preconditioning temperatures. The temperatures of CIW increased from west to east, in line with the sea surface temperature gradient. Notably, thicker and colder CIW was found in the western cyclonic gyre compared to the eastern cyclonic area. Furthermore, the study confirms that the warming trend in CIW, identified in previous research, not only continues but has intensified during the recent period analyzed. These findings, observed under the extreme conditions analyzed in this research, offer valuable insights into the widespread occurrence of CIW formation in the Black Sea. Additionally, the study confirms that the warming trend in CIW, identified in previous studies, continued in the region throughout the warm winter period and after the cold spell in 2022. These insights contribute to a deeper understanding of CIW dynamics and their response to extreme weather events in the Black Sea.

Keywords: CIL; CIW; Black Sea; cold episode; SST; SST; SLA

Citation: Çokacar, T. Cold Intermediate Water Formation in the Black Sea Triggered by March 2022 Cold Intrusions. *J. Mar. Sci. Eng.* **2024**, *12*, 2027. https://doi.org/10.3390/jmse12112027

Academic Editor: João Miguel Dias

Received: 14 August 2024
Revised: 31 October 2024
Accepted: 6 November 2024
Published: 9 November 2024

1. Introduction

In mid-March 2022, a Siberian High, accompanied by intense cold air masses, resulted in challenging weather conditions over the Western Black Sea. According to the Copernicus Climate bulletin, March 2022 exhibited colder-than-average conditions in southern Europe, with the most significant cold anomalies observed in Turkey and Greece "https://climate.copernicus.eu/surface-air-temperature-march-2022 (accessed on 2 June 2023)". The outbreaks of cold air eastward from this Siberian High pressure system led to frequent cold spells in the northern and western regions of the Black Sea [1–4]. Episodes of strong cold air incursions induced high heat fluxes across the sea surface and caused a decrease in surface temperatures [3–9].

A stable two-layer stratification is present in the Black Sea, where the surface layer, extending to approximately 150 m, is sensitive to atmospheric conditions. The Rim Current, the main cyclonic current flowing along the continental slope, involves cyclonic gyres inside and anticyclonic eddies broadly at its peripheries [8,10,11]. Convection driven by strong winter cooling from cold intrusions forms the cold intermediate water (CIW)

mass. Trapped between the permanent pycnocline and the seasonal thermocline, this cold mass spreads across the basin, creating a distinct boundary layer that separates surface waters from deeper ones. Known as the cold intermediate layer (CIL), it is conventionally identified by temperatures below 8 °C. Although there is growing consensus on how the CIL forms in the Black Sea, its formation and evolution is not entirely understood. The most common explanation for CIL formation involves two processes. The first is winter convection occurring in the center of cyclonic gyres, spreading along the isopycnals toward the periphery [12–14]. The second involves the horizontal flow of cold-water masses from the Northwestern Shelf (NWS) to the adjoining slope region, followed by their distribution across the basin through the Black Sea Rim Current [12–14]. Numerical modeling studies examining the contributions of various regions to CIL formation emphasize the prominent role of the NWS continental slope, followed by the cyclonic interior region [14,15]. Extensive research has explored the process of CIL replenishment, its interaction with dynamics, and its inter-annual variability [1,3,5,9,12,15–18]. Despite the Black Sea experiencing a warming trend in sea surface temperature (SST) since the 1900s, a CIL warming trend exceeds this surface trend, and the CIL is at risk of disappearing [19,20]. Winter convection plays a crucial role in forming the cold intermediate layer, transporting oxygen-rich surface water into the subsurface [5,20,21]. However, the complex processes behind the formation and evolution of the CIL require further analysis to fully understand and assess Black Sea water mass dynamics [5,15,16,18,22]. A deeper understanding of CIL renewal is also essential for clarifying the ecosystem dynamics of the Black Sea [15,23–25].

This study aims to enhance our understanding of CIL formation and its spreading by analyzing Argo float data during the anomalously cold episodes in March 2022, which triggered convective mixing in the upper water column of the Black Sea. The findings provide distinct evidence of extensive CIL replenishment in the Black Sea. Section 3 examines the March 2022 cold outbreaks, while Section 4 analyzes ocean reactions and CIL formation through the cold episodes. Section 4.1 examines long-term winter SST changes from 2000 to 2022, during which 2020 and 2021 were recorded as having the two warmest winters. The variations in SST and heat flux before, during, and following the cold episodes from January to April 2022 were evaluated. Section 4.2 evaluates CIW formation throughout the consecutive March 2022 episodes, analyzing temperature and salinity in the top 120 m of the water column by means of the evaluation of heating/cooling processes and surface dynamics at the position of the floats. In Section 4.3, Argo float data are utilized to provide monthly insights into the basin-wide evolution of CIL.

2. Data and Methods

SST analyses relied on regional data products provided by the Copernicus Marine Environment Monitoring Service (CMEMS). The reprocessed Black Sea SST dataset (https://resources.marine.copernicus.eu/product-detail/SST_BS_SST_L4_REP_OBSERVATIONS_010_022/INFORMATION) was accessed on 2 June 2023. BS SST products are constructed through the reprocessing of collated Level-3C (merged single-sensor, L3C) climate data records provided by the ESA Climate Change Initiative (CCI) and the Copernicus Climate Change Service (C3S) initiative and also include an adjusted version of the AVHRR Pathfinder dataset [26,27]. The daily night-time SST fields integrated through an optimal interpolation scheme are received on a 1/20° regular grid. SST anomalies were calculated from the 22 years' climatological means of Copernicus Rep BS SST. SST anomalies were obtained by taking the difference between daily SST and the climatological SST.

Sea-level anomaly (SLA) and geostrophic velocity data were extracted from the gridded sea surface height data for European seas provided by CMEMS (https://resources.marine.copernicus.eu/product-detail/SEALEVEL_EUR_PHY_L4_MY_008_068/INFORMATION, accessed on 2 June 2023), which derived from the optimally interpolated along-track data from various altimetry missions. Atmospheric forcing was received from the European Centre for Middle-Range Weather Forecasts (ECMWF) ERA5 reanalysis (https://cds.climate.copernicus.eu/datasets/reanalysis-era5-single-levels?tab=overview, accessed on 2 June

2023). Geopotential height anomalies were calculated using 32 years' (1990–2022) monthly ERA5 geopotential reanalysis data. In addition, the ERA5 daily mean surface heat flux was calculated using hourly surface heat flux reanalysis data. It was used to estimate the degree of winter cooling. The Argo program for ocean monitoring provides regular measurements for the temperature and the salinity of a water column of 500–1550 m with 1 m bins once a week. The accuracies of the float data were concluded to be 0.002 °C for temperature, 2.4 dbar for pressure, and 0.01 PSU for salinity, after delayed-mode adjustments [28,29]. The Argo data were obtained from ftp://ftp.ifremer.fr/ifremer/argo. Six Argo floats were chosen for tracking the dynamical changes in the water column. Both surface current and sea surface height anomalies were extracted along Argo float trajectories by selecting the closest grid data to the Argo position from the Copernicus data. Argo float data were complemented by the sea mean CIW temperature. The mean CIW temperature and salinity were calculated with the criterion of temperatures less than 8 °C. The Argo float IDs used here are provided in Table 1 (see also http://marine.copernicus.eu/, accessed on 2 June 2023). The total number of available active Argo floats was 21 in 2020 and 2021 and 13 in 2022.

Table 1. The Argo float IDs active in the Black Sea and grouped according to the analysis intervals considered in this study.

Dates	Argo Float ID
1 January 2020–31 December 2022	3901852, 3901854, 3901855, 3902004, 3902005, 3902006, 4903711, 5906866, 6901832, 6901833, 6901834, 6903240, 6903271, 6903766, 6903782, 6903866, 6903867, 7900591, 7900595, 7900596, 7901065
1 January 2022–8 May 2022	3901852, 3901854, 3901855, 3902004, 3902005, 6903240, 6903271, 6903766, 6903782, 6903866, 6903867, 7900595, 7900596

3. Synoptic Atmospheric Conditions

The first episode of cold Siberian air masses affecting the Black Sea occurred on 9–11 March in 2022, induced by a jet stream excursion through its northwest. Following a one-week interval, the second cold episode, accompanied by a high-pressure system, became effective in the region between 18 and 20 March. Consequently, geopotential anomalies made a sharp transition from −30 m to +90 m in ten days, mainly over the Western Black Sea basin (Figure 1a,b). Eventually, the winds strengthened in the area, in line with the increase in the gradient of geopotential anomalies during the cold episodes. The daily mean air temperatures, wind, and geopotential height anomalies at 850 mbar on 10 and 18 March are shown in Figure 1a,b.

The gradual decrease in air temperatures at the beginning of March was followed by a sudden drop, reaching 0 °C on March 11th, with a sharp decrease of approximately 6 °C within just a few days (Figure 1e). In the course of the first episode on 9–11 March, the mean wind speed at sea level was around 11.2 m/s, blowing from the north (Figure 1d). Then, the mean atmospheric pressure rose to 1034 mbar in a couple of days (Figure 1e). The subsequent cooling episode on 17–20 March led to a second minimum in air temperatures and strengthened the wind again. In sum, the cold and stormy weather intrusions prevailed for more than 10 days in the Black Sea.

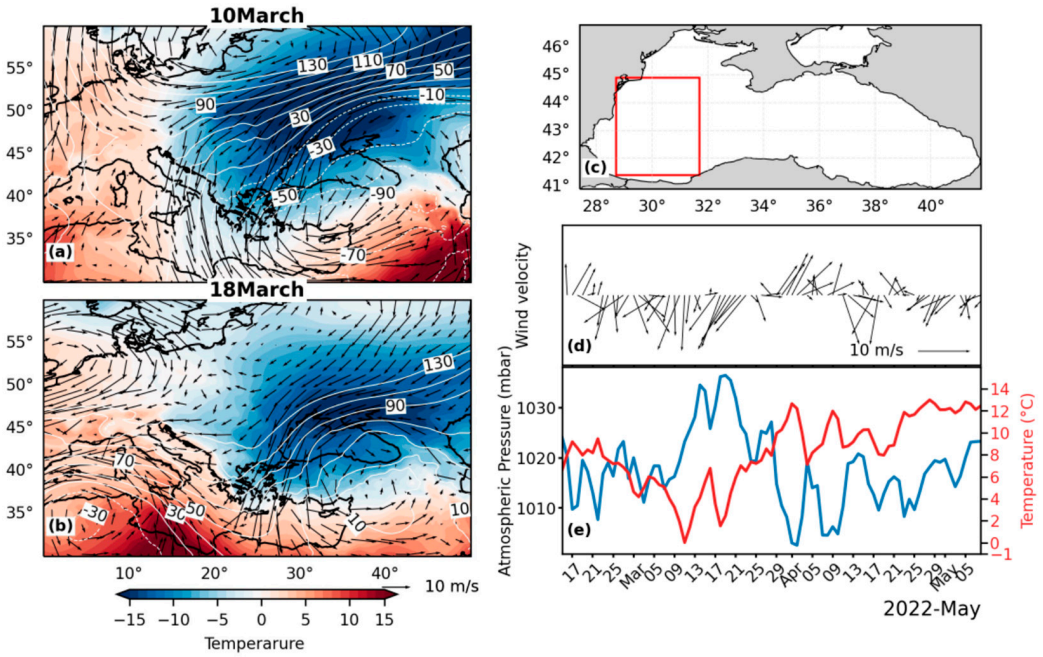

Figure 1. ECMWF ERA5 data for (**a**) 10 March and (**b**) 17 March at 850 mbar daily mean air temperatures (color), wind (arrows), and geopotential height anomalies (white contour lines) calculated based on monthly climatology for the period 1990–2022. (**c**) The selected area for calculating the means (shown with red box): (**d**) mean wind at sea level (oceanographic convention); (**e**) mean pressure (blue line) and atmospheric temperature (red line) at sea level in the selected rectangular area. The means were calculated for the selected rectangular area (**c**) on the Western Black Sea by taking into consideration that the episode was more pronounced in the Western Black Sea.

4. Ocean Reaction

4.1. Surface Signature

The long-term temperature variations in the Black Sea indicate two distinct phases marked by decadal oscillations: a cooling phase from 1960 to 1993, followed by a warming phase that began in 1993 and continued thereafter [1,25,30,31]. The decadal oscillations are primarily influenced by the North Atlantic oscillation (NAO) and shorter oscillations associated with the East Atlantic/West Russia (EA-WR) oscillation [1,25]. The warming trend in SST and CIL temperatures from 1993 to 2013 was shown in [16]; the SST trend was extended until 2022 in this study. Figure 2a illustrates the persistent warming trend (0.39 °C per decade), with the mean winter SST reaching 10.01 °C in 2020 and 9.99 °C in 2021, marking exceptionally warm years for 2000–2022. Notably, the 10.01 °C recorded in 2020 stands as the highest winter SST since the 1960s, surpassing the previous peak of 9.75 °C in 1963 [16].

A larger timeframe, starting from 2019, is necessary for analyzing the ocean reactions to March 2022 cold episodes, as the CIL retains a memory of atmospheric conditions from previous winters [17,18]. In 2020 and 2021, mean SSTs consistently exceeded 8 °C; in February 2022, these dropped slightly below 8 °C, reached 7.90 °C, and finally decreased down to 7.58 °C following the two consecutive episodes in March 2022 (Figure 2b). To understand the prevailing conditions in the Black Sea prior to the cold intrusions of 2022, SST and surface heat fluxes were analyzed starting from early 2019. In 2022, SST dropped below 8 °C after two warmer years. In the beginning of February 2022, the temperature dipped slightly below 8 °C, reaching 7.90 °C, and eventually dropped to 7.58 °C following two consecutive cold episodes in March 2022, as indicated by the red shading in Figure 2b. The winter SST decline was a response to increased heat loss, where the basin-wide daily mean heat flux reached up to -400 W/m^2 (Figure 2c). Following the winter cooling, cold intrusions in March triggered a second peak in heat loss, with fluxes reaching approximately

-250 W/m^2. The lowest SST was observed in March 2022 during the Siberian cold episode. Figure 2d–g display the monthly mean SST maps. The spatial variations in SST are linked to the distribution of heat content and the local dynamics, characterized by cyclonic circulation dominating the basin's interior and anticyclonic eddies meandering around the periphery of the Rim Current [31]. The coldest temperatures were observed in the shallow, less saline waters of the NWS region throughout all seasons. Figure 2d shows that in January, the coldest temperatures were confined to the NWS area. In February, temperatures below 8 °C expanded into the interior cyclonic area and the western half of the basin (Figure 2e). By March, cold outbreaks significantly intensified the surface heat loss, leading to a pronounced basin-wide drop in SST, with the temperatures below 8 °C expanding across the basin, except in the northeastern region (Figure 2f). However, by April, this cold area became restricted to the NWS with the onset of seasonal warming (Figure 2g).

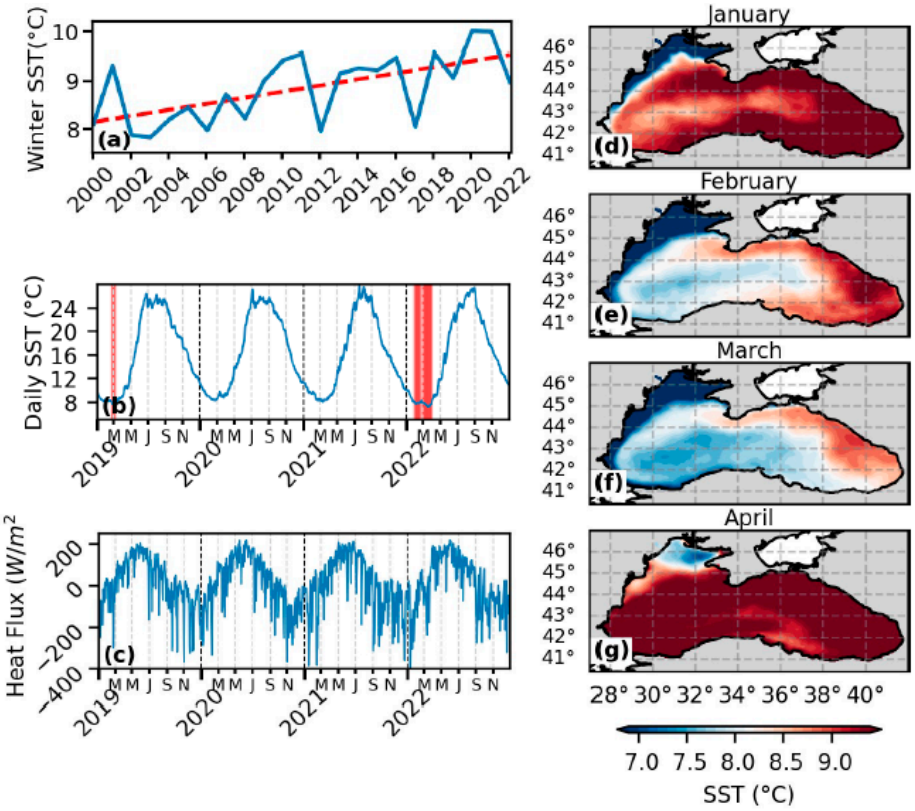

Figure 2. (**a**) Inter-annual variations in the basin-wide winter (December–March) mean SST, calculated from the Copernicus CMEMS gridded BS-SST product data (2000–2022), with the red dashed line representing the trend. (**b**) Daily SST variations for 2020–2022, where red shaded columns indicate values below 8 °C. (**c**) Variation in basin-wide daily surface heat flux, calculated from ERA5 data for 2019–2022. Surface monthly mean SST values for 2022 are shown for (**d**) January, (**e**) February, (**f**) March, and (**g**) April, obtained from the Copernicus CMEMS gridded SST product.

Figure 3a,c,e display the SST anomalies' (SSTAs') distribution along with SST contours for selected dates during the first and second episodes, as well as during the subsequent period. On March 10, the coldest waters on the Northwestern Shelf and along the western and southern coasts gradually moved eastward, following the periphery of the Rim Current. Simultaneously, the cyclonic circulation of the Rim Current transported relatively warmer water westward from the east [4,8,10]. By the second episode on March 18 and in the following period, SST decreased further, and cold anomalies intensified.

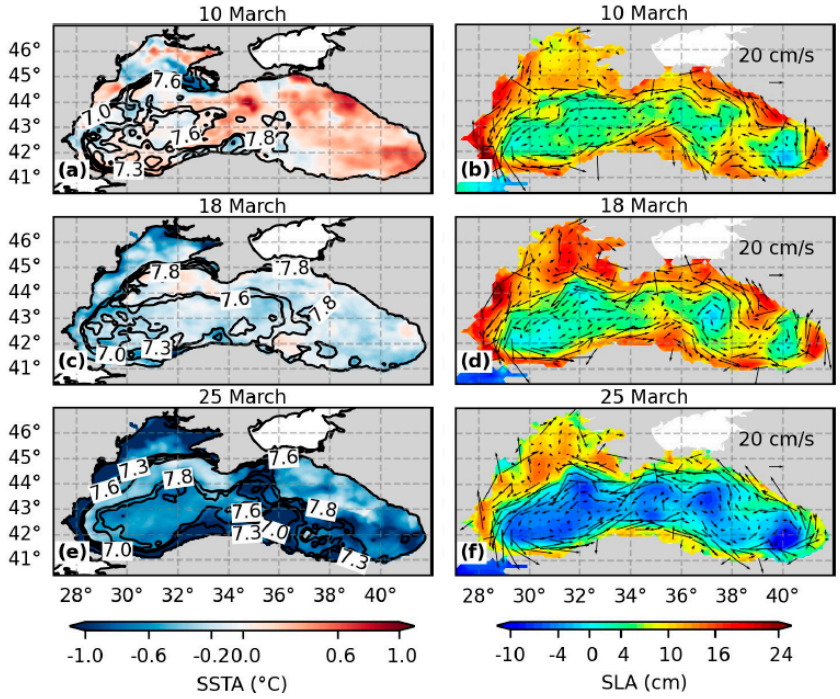

Figure 3. SSTA values calculated from the Copernicus CMEMS gridded BS-SST product based on the SST climatology (2000–2022) shown for (**a**) 10 March, (**c**) 18 March, and (**e**) 25 March, with the 8 °C SST highlighted by a black contour line over the SSTA. Meanwhile, SLAs are shown for the same dates in (**b**,**d**,**f**), where SLAs and geostrophic currents, obtained from Copernicus CMEMS gridded sea surface height data, are represented by arrows indicating geostrophic velocities.

Evaluating the spatio-temporal SSTA for March 2022, Figure 3a reveals a noticeable gradient in SST, as well as in SSTA, which increases from west to east over the first episode. The SST gradient aligns with the climatological monthly means in March [32]; however, the intrusion of cold air from the west resulted in a cooler SST in the western basin when compared to the climatological mean temperatures. The sharp gradient in SSTA, during the first intrusion, was reduced by the second episode (Figure 3c). In the next couple of days, negative anomalies were extended across almost half of the basin. Throughout the first cold episode, cooling was primarily effective in the western basin, whereas for the second episode, together with the local circulation dynamics, cooling was effective all over the basin. This second episode resulted in a substantial change, with negative SSTA across the entire basin and an additional ~0.3 °C decrease in SST (Figure 3c). Following the second episode, SSTA rose up to −1 °C along the periphery in the western and southern regions of the Black Sea (Figure 3e).

SLA fields are displayed in Figure 3b,d,f. The circulation structure is characterized by a narrow Rim Current that includes two decoupled gyre systems, which became separated at approximately longitude 38° (Figure 3b). The western cyclonic gyre system was extending to southeastward, covering most of the basin and consisting of three mesoscale cyclonic gyres within it. These cyclonic gyres appear to have been strengthened by the second cold episode (Figure 3d). Flow at the narrow channel separating the southeastern cyclonic gyre from its larger counterpart weakened (Figure 3d). The meandering Rim Current was intensified by the second cold intrusion, where the Rim Current jet flow exhibited varying velocities, reaching 50–70 cm/s in the west and up to 100 cm/s in the southwest section (Figure 3d). Indeed, these velocities corresponded to the highest climatologic geostrophic velocities of the Rim Current [3,9]. Finally, during the subsequent period, the Rim Current developed into a continuous, basin-wide cyclonic system (Figure 3f). This system involved all four gyres, which became interconnected. The western gyre extended to around 34°N, while the other three gyres were positioned in the interior half of the basin, forming a

continuous cyclonic system. The anti-cyclonic eddies over the Rim Current periphery began to weaken (Figure 3f).

Anticyclonic eddies intensified by the second episode, caused a drastic drop in SLAs in the entire interior cyclonic area. Positive high sea-level anomalies (~8 cm) in the cyclonic interior area (Figure 3b) dropped to ~−10 cm (Figure 3f). The intense circulation period observed from March 17 to 25 had gradually diminished by the end of the month.

4.2. Vertical Structures and CIW Formation

In order to evaluate the vertical structures in the uppermost water column, 5 Argo floats were selected out of 13 active floats over the Black Sea in 2022 (Figure 4a). The trajectories of the selected floats (3001854 across the north to southwest, 3902005 in the south along the southern Rim Current zone, 6903867 and 690366 in the central zone, and 7900595 in the southeast Black Sea) provided good coverage which dynamically resembled different areas in the Black Sea (Figure 4a). Integrated time variations in temperature compiled from floats were examined against both depth and density coordinates. The time window size was kept larger to capture the abrupt changes in water column temperature and stability during the cold events. Considering the spatial variability of the Argo floats within this time window, SLAs and heat flux were specifically evaluated at the float positions to account for the local dynamics.

The yellow frame in Figure 4b–m highlights two successive cold episodes and following intense dynamic periods. Over this timeframe, there was a simultaneous decrease in upper layer temperatures (<8 °C) observed for all floats, as depicted in Figure 4d–m. The SLAs and surface heat fluxes extracted along Argo float trajectories are depicted in Figure 4b,d. The extracted heat fluxes showed two minima, one in January and the other in March. The heat loss over the prevailing warm waters in January did not result in any CIW formation. However, the relatively weaker March episodes led to significant cooling in the mixed-layer water column. The SLA indicated a sharp transition from +17 cm to −17 cm over a two-week period within the highlighted yellow timeframe. The notable decreasing gradients of SLAs and heat flux were observed during the second episode. The maximum cooling in March, within the marked yellow timeframe, reached 250 W m^{-2} and was observed at the positions of Argo floats in the northwestern Rim Current zone, followed by the interior cyclonic area, with weaker cooling in the southern periphery.

In February, Argo float 3901854 travelled along the northeastern edge of the Rim Current (Figure 4d,e), where the upper-layer temperatures were above 8 °C. As shown in Figure 2e, the temperatures in the northeastern region were higher than those in the northwestern part because of the advection of warmer waters from the east by the Rim Current [8,10]. Argo float 3901854 travelled to the edge of the NWS in the cold-episode period. The float recorded temperatures under ~8 °C in this area over the first event. When the second cold episode occurred, the float was still in the north and drifting on the continental slope of the NWS close to the anticyclonic eddy formed in the NWS, as seen from SLA maps on 18 and 25 March (Figure 3d,f). Previous modelling efforts and observations demonstrated that the northwestern cross-shelf area was a major contributor to the CIW formation by transporting the cold NWS waters isopycnally to the deep interior [9,12,14,33]. When less saline and low-temperature waters of the northwestern shelf mixed with saline waters of the open interior, the density increased. That density increase caused cold-water penetration deeper into the water column. The anticyclones formed along the edge of the NWS, continually fed by cold waters from the coastal shelf, enhanced deep convection. After the second episode, Argo float records depicted a drop from 7.9 °C to 7.3 °C in the upper 50 m (Figure 4d) accompanied by cold-water intrusion to a denser layer of 15.0 σ_t (Figure 4e). The convective mixing shifted the lower boundary of the CIL remarkably at the 14.75 σ_t to 15.0 σ_t isopycnal surfaces. In mid-April, the thickness decreased to ~25 m, with a temperature of ~7.75 °C. The CIL temperature gradually increased during April and May as the float drifted southwest along the Rim Current.

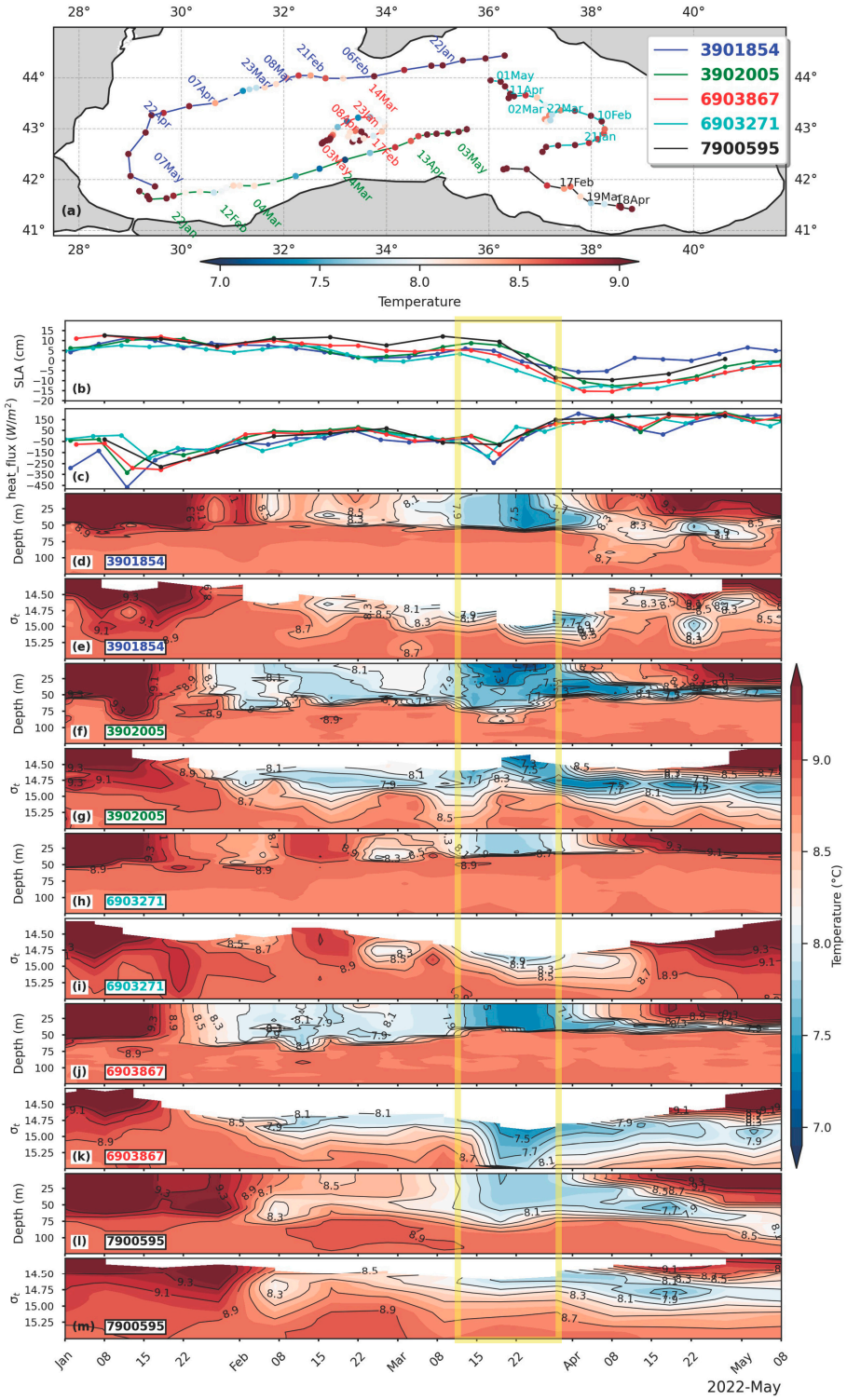

Figure 4. (**a**) Tracks of chosen Argo floats between February and May 2022. Colors of the circular position markers show the Argo sea surface temperatures. (**b**) SLAs for each float (color) were plotted by extracting the Copernicus CMEMS grids closest to the float locations. (**c**) Daily mean surface heat flux, derived from ERA5, along float trajectories. Subfigures (**d**,**e**) 3901854, (**f**,**g**) 3902005, (**h**,**i**) 6903271, (**j**,**k**) 6903867, and (**l**,**m**) 7900595 show the surface to 125 m and 15.5 σ_t-level temperature contours of the Argo floats. The missing values in the contour plots of temperature variations versus σ_t in time arose from changes in the σ_t range during the cooling period, where a decrease in surface column temperature caused an increase in the density of the surface thin layer. The yellow frame highlights two successive cold episodes and following intense dynamic period.

The float 3902005 was on the southwestern Black Sea drifting along the Rim Current flow direction until the end of March; then, its path was altered to the interior basin in April. In January, near Bosporus, the float recorded mixed-layer temperatures above 9.3 °C. By the end of January and February, the mixed-layer temperatures were around 8 °C, yet the layer was not completely homogeneous (Figure 4f,g). Following the first episode on 9–10 March, the mixed-layer temperatures dropped to 7.5 °C. Over the second episode between 17 and 20 March, a sharp decrease in SLAs (Figure 4a) and strong geostrophic flows (~60 cm/s) at 3902005's positions (Figure 3d) indicated intense dynamics. The mixed layer deepened to nearly 60 m coincident with the sharp decrease in temperatures, suggesting that the deepening was a result of convective mixing in addition to local dynamic circulation accompanied with enhanced Rim Current flow (Figure 3f). Stratification was established as air temperatures rose, and the uppermost 25 m layer warmed by the end of March. A newly formed CIW, located between 25 and 60 m, decreased to 50 m when the float changed its path to the interior basin in April. Apparently, the 8 °C isotherm rose from 14.75 σ_t to ~15 σ_t in the cyclonic interior part (Figure 4g).

Argo floats 6903271 and 6903867 were in the eastern and western cyclonic interior, respectively. Figure 4h,i show that the upper-mixed-layer temperatures were slightly cooler than 8 °C in the eastern basin during the cold-episode period depicted by the yellow frame. It should be noted that the eastern basin had a higher SST than the western gyre (Figure 3a,c,e). Although the temperature of the mixed layer decreased remarkably—about 0.7 °C throughout two consecutive episodes—the temperatures in the uppermost 50 m decreased down to 7.9 °C (Figure 4h,i) due to the high background temperatures in the eastern basin. The 8 °C temperature of the CIL definition was only met during the time interval between two episodes in the eastern basin. Figure 3b,d,f reveal that the western gyre extended eastward, comprising various cyclonic structures at different scales. Float 6903867 drifted within this elongated western cyclonic gyre (Figure 4a), following a cyclonic eddy pattern in the mid-latitudes. In February, temperatures in the quasi-homogeneous layer (~60 m) dipped slightly below 8 °C (Figure 4j). The intensification of cyclonic circulation resulted in a pronounced "doming" of the isopycnal surfaces, as noted in many studies [9,16]. In other words, the upwelling of relatively dense deep waters reduced the static stability of the surface layer above the pycnocline. In the Western Black Sea, the Rim Current became more intense, starting with the first episode and gaining strength with the second episode (Figure 3b,d,f). This intensification of the Rim Current led to noticeable "doming" and resulted in shoaling of density layers, reducing the pycnocline from ~48 m in early March to ~38 m (Figure 5a). The second episode led to further cooling of the mixed layer to ~7.3 °C, which was the minimum temperature recorded on the western cyclonic gyre. The convective mixing eroded the upper pycnocline by allowing cold surface water to enter deeper isopycnal levels, as indicated by the steep gradient lines framed with a yellow box in Figure 4k. By the subsequent seasonal surface warming, the thermocline was formed; meanwhile, the density at the lower boundary of the 8 °C isotherm decreased from 15.50 σ_t to ~15.25 σ_t (Figure 4k). In April, the cold-water mass was confined between the seasonal thermocline and the permanent pycnocline and formed a thin CIW with a 20 m thickness (Figure 4j,k). The temperature of this CIW increased in time due to mixing of the cold-water mass with the upper thermocline waters and outcropping of the pycnocline. A detailed analysis of the CIW formation in the cyclonic interior is provided in the following T-S diagram analysis in this section.

Argo float 7900595 drifted over the southeastern zone of the Rim Current (Figure 4a). The temperature of the upper mixed layer, initially at 8.5 °C at the beginning of March, dipped slightly below 8 °C during the first cold episode and further decreased to 7.7 °C with the second episode later in March (Figure 4l,m). The float followed the Rim Current as it meandered around the anticyclonic eddy in the southern periphery area between longitudes 37° and 39° (Figure 3b,d). Because the weaker stability in the anticyclonic area allowed deeper ventilation [14,16], cooling extended up to ~75 m. After spring warming, the temperature rose and the thermocline formed, deepening to 60 m by the end of spring

(Figure 4l). The cold layer under the thermocline, between depths of 25 m and 50 m, warmed but remained under 8 °C at the end of April (Figure 4l).

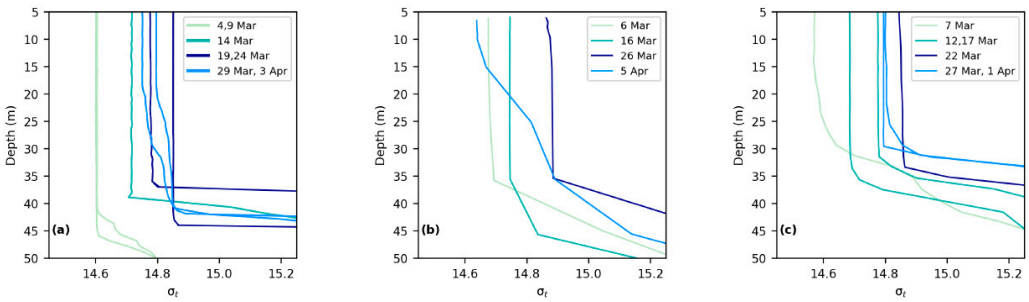

Figure 5. Change in σ_t with depth during cold episodes as sampled by Argo floats drifting inside cyclonic interiors: (**a**) 6903867 in the western zone; (**b**) 7900596 in the central zone; (**c**) 6903271 in the eastern zone. The plots indicate measurements between 4 March and 5 April for the respective zones.

Figure 6 shows temperature–salinity (T-S) diagrams for the period corresponding to the two consecutive cold episodes. This period is indicated with a yellow frame in Figure 4b–m. Please note that 12 out of 13 active Argo floats in the Black Sea are plotted (only float 6903782 is not, because it travelled from an anticyclone to a cyclone). The trajectories of these floats covering the analysis period are indicated in the Supplementary Materials, Figure S1. Due to lower current speeds in the cyclonic interior, the floats drifted short distances and stayed relatively stationary inside gyres. Therefore, the time window could be made wider in the interior cyclonic area, covering the period from 1 March to 5 April 2022 (Figure 6a–c). On the other hand, the time window was made narrower for the Rim Current and its periphery area, since the high current speeds associated with the Rim Current lead to significant drifting of floats. Moreover, other factors, such as dynamic features and mesoscale coastal eddies in the narrow band of the continental shelf, introduced complexity into the analysis. Consequently, a limited time window for evaluations was necessary to eliminate the influence of local dynamics at the new position of a float. Therefore, a shorter time window was selected, and two consecutive measurements were analyzed through the coldest period in these areas. The lowest temperatures observed between March 14 and 25 were analyzed (Figure 6d).

Figure 6a–c show T-S diagrams in the cyclonic interior in the order of positions of the floats from west to east. All of the three floats (Figure 6a–c) showed effective cooling after the first episode (on 12, 14, 15, and 17 March), as indicated in dark green. The measurements just after the second episode period (12–24 March) are shown in dark blue. It was observed that the eastward depth inclination of convection matched the background temperature profiles of the three subregions in the cyclonic interior. In fact, the temperature drop (in the upper mixed layer) during the two consecutive episodes was almost the same (~0.7 °C) in all the three float measurements in the cyclonic interior; this occurred independently of the measurement location. The salinity of the mixed layer gradually increased in the first episode and continued until the second episode. After the second episode, all three floats in the cyclonic interior showed a strong increase (>0.2 ppt) in mixed-layer salinities (Figure 6a–c). The mixed-layer depth decreased gradually in the western gyre with the initiation of the first episode until the end of the second episode. Figure 5a depicts the shoaling of the mixed-layer depth (from 47 m to 39 m on 14 March) with the first cold intrusion and its further reduction to 36 m with the second cold intrusion on 19 March. The increase in the mixed-layer salinity (~0.2 ppt) and its accompanying density can be explained by the weakening of the static stability at the pycnocline due to upwelling. As the intensity of circulation weakened after the second episode, the mixed layer deepened to 45 m on 24 March (Figure 5a), the mixed-layer temperature decreased to its minimum, and its salinity continued to increase. Over 5 days, the salinity of the mixed layer increased by 0.08 ppt, while the temperature dropped by approximately 0.1 °C (Figure 6a), indicating convective mixing. As surface heat loss made the water cooler and denser, it sunk into the

deeper, more saline waters, leading to a corresponding increase in the salinity of the sinking water. Following the second episode, the salinity of the newly formed CIW increased by ~0.2 ppt in total compared to the beginning of March; this was accompanied by an increase in σ_t of about 0.25: from ~14.6 to ~14.85 (Figure 6a).

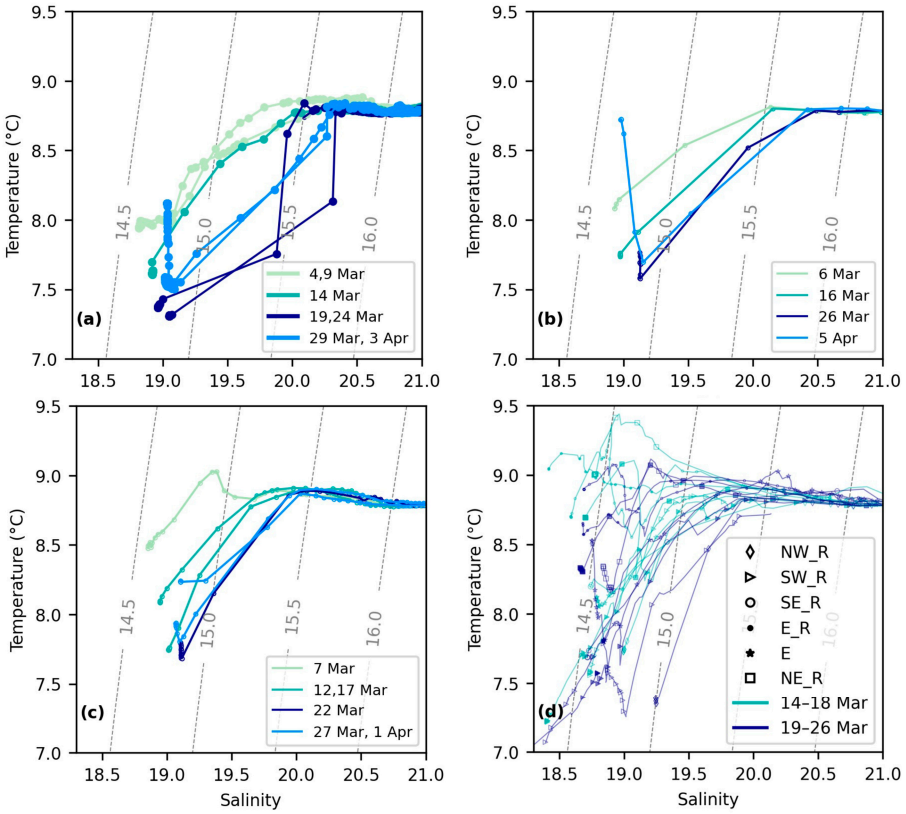

Figure 6. T-S graphics for cold episodes sampled by Argo floats drifting inside the cyclonic interior: (**a**) 6903867; (**b**) 7900596; (**c**) 6903271. The plots cover the period of measurement between 4 March and 5 April. Light green lines correspond to the dates prior to the first episode, while dark green lines correspond to the dates between the two episodes, and dark blue lines show the period affected by the second episode. Lastly, light blue lines indicate the initiation of the seasonal warming period. (**d**) T-S graphics during cold episodes sampled by Argo floats drifting along the Rim Current (west) and periphery. The subfigure covers the period of measurement between 14 and 26 March, where measurements for 14–18 March are shown in dark green and those for 19–26 March are shown in dark blue. Argo float 3901854 in the northwestern Rim Current ("NW_R") is denoted by diamonds, and measurements of Argo floats 3901855 and 3901852 in the northeastern Rim Current ("NE_R") are denoted by hollow and filled squares, respectively; measurements of 3902004 and 3902005 in the southwestern Rim Current ("SW_R") are denoted by hollow and filled triangles, respectively; measurements of 7900595 in the southeastern Rim Current ("SE_R") are denoted by circles; measurements of 6903240 and 6903766 in the eastern Rim Current ("E_R") are denoted by hollow and filled dots, respectively; and measurements of 6903866 in the eastern part ("E") are denoted by stars.

Figure 5 presents the density profiles obtained from Argo floats drifting through three cyclonic structures within the Rim Current: the western, mid, and eastern zones centered at 34° E, 35° E, and 37° E, respectively. As explained in Section 4.1 and illustrated in Figure 3b,d,f, the sea level dropped due to the intensification of the Rim Current within the cyclonic interior during the cold episodes. The mixed-layer depth in the western cyclone shoaled over the cold episodes and then deepened afterward (Figure 5a). In contrast, the mixed layers in the central and eastern cyclones remained stable at around 35 m throughout March (Figure 5b,c). According to the discussion in Section 4.1, the difference between

the western gyre and the central and eastern gyres can be attributed to relatively weaker upwelling and less intense circulation in the latter through the cold episodes. Additionally, the increase in upper-mixed-layer salinity corresponded to the decrease in temperatures observed on 16 and 26 March (Figure 6b) and on 12, 17, and 22 March (Figure 6c).

Figure 6d shows T-S diagrams of the floats drifting along the Rim Current and its periphery by indicating the locations of the floats during 13–25 March as the northwestern, "NW_R"; southwestern, "SW_R"; southeastern, "SE-R"; eastern, "E_R"; and northeastern, "NE_R" part of the Rim Current and eastern periphery "E". The measurements made just after the second intrusion, shown in dark blue, were saltier than the previous measurements for all floats. The northwestern part of the Rim Current was particularly notable for its ~0.3 ppt increase in salinity, ~0.25 increase in σ_t (15 σ_t), and additional temperature decrease of ~0.3 °C within a couple of days after the second episode. It was observed that the temperature increased gradually clockwise along the Rim Current and in the southwestern part of the Rim Current; the deepening occurred from 14.5 σ_t to 14.6 σ_t. In the southeastern part, it deepened from 14.70 σ_t to 14.80 σ_t (Figure 6d). The greatest temperature drop was observed in the northeastern part of the Rim Current. Although cooling was strong, relatively high temperatures were noted in the upper water. This phenomenon resulted from the advection of warm waters from the eastern zone of the Rim Current, preventing convection to very deep waters [14]. In other words, as the cooled-down surface water mixed with the warm water carried by the Rim Current flow, the CIW formation rates were reduced by local dynamics. Precisely the opposite situation was observed in the Western Black Sea, where the Rim Current (Figure 6a) transported cold water originating from the northern shelves into a narrow band over the continental slope. The advection of the water column along the Rim Current preconditioned the penetration of surface cooling down to deep layers. No convection was observed in the northeastern periphery area.

4.3. Evaluation of CIL

All cycles of active Argo floats, covering 2022, as well as the two preceding warm years, are shown in Figure 7. Cycles with a mean temperature of the water column below 8 °C are shown as blue circles; darker blue tones represent colder temperatures, while circle size indicates the thickness of the cold layer. Orange circles indicate water column temperatures between 8 °C and 8.5 °C, which are near the CIL boundary temperature definition.

A total of 21 Argo active floats provided a good areal distribution of measurements in a total of 1534 cycles throughout the warm years of 2020 and 2021 (Figure 7a,b). In these years, only a few instances of a thin layer (<7 m) were recorded in February and March, with temperatures slightly cooler than 8 °C. The cooling events, however, were not sufficiently strong to create deep convection. Hence, the CIL detections were rare and limited to the northwestern continental slope and cyclonic gyres during this period. The annual mean SST distribution, which remained above 8 °C across the entire basin except for the western shelf area (Supplementary Materials, Figure S4), strongly suggests that CIL formation was rare in the entire basin over these years. Therefore, by early 2022, there was no old CIL remaining from previous years. This situation provided a unique opportunity to directly observe the formation and spread of a new CIW mass.

In January 2022, surface heat loss intensified due to cooling events (Figure 2c), but it was not strong enough to lower surface temperatures below 8 °C. However, a few Argo floats recorded temperatures below 8.5 °C in the eastern and southern Black Sea (Figure 7c). In February, gradual cooling affected the entire basin, with temperatures increasing from west to east (Figure 2e). During this period, the upper-mixed-layer temperatures fell slightly below 8 °C in the cyclonic interior and near the Bosporus area (Figure 7d).

The most extensive, thickest, and coldest water formation occurred in March (Figure 7e) and was driven by episodic cold intrusions discussed in Section 3. It was widespread, excluding the northeastern part of the Rim Current and its peripheries. Argo floats in the Western Black Sea recorded CIL temperatures as low as ~7.3 °C, while floats in the eastern region registered warmer CIL temperatures, indicating an increase in CIL temperatures

from west to east. No CIL was observed in the northeastern part of the Rim Current, while it was present in the northwestern section. The relatively warm waters advected from the eastern Rim Current could explain the absence of CIW in the northeastern Rim Current near the Kerch Strait.

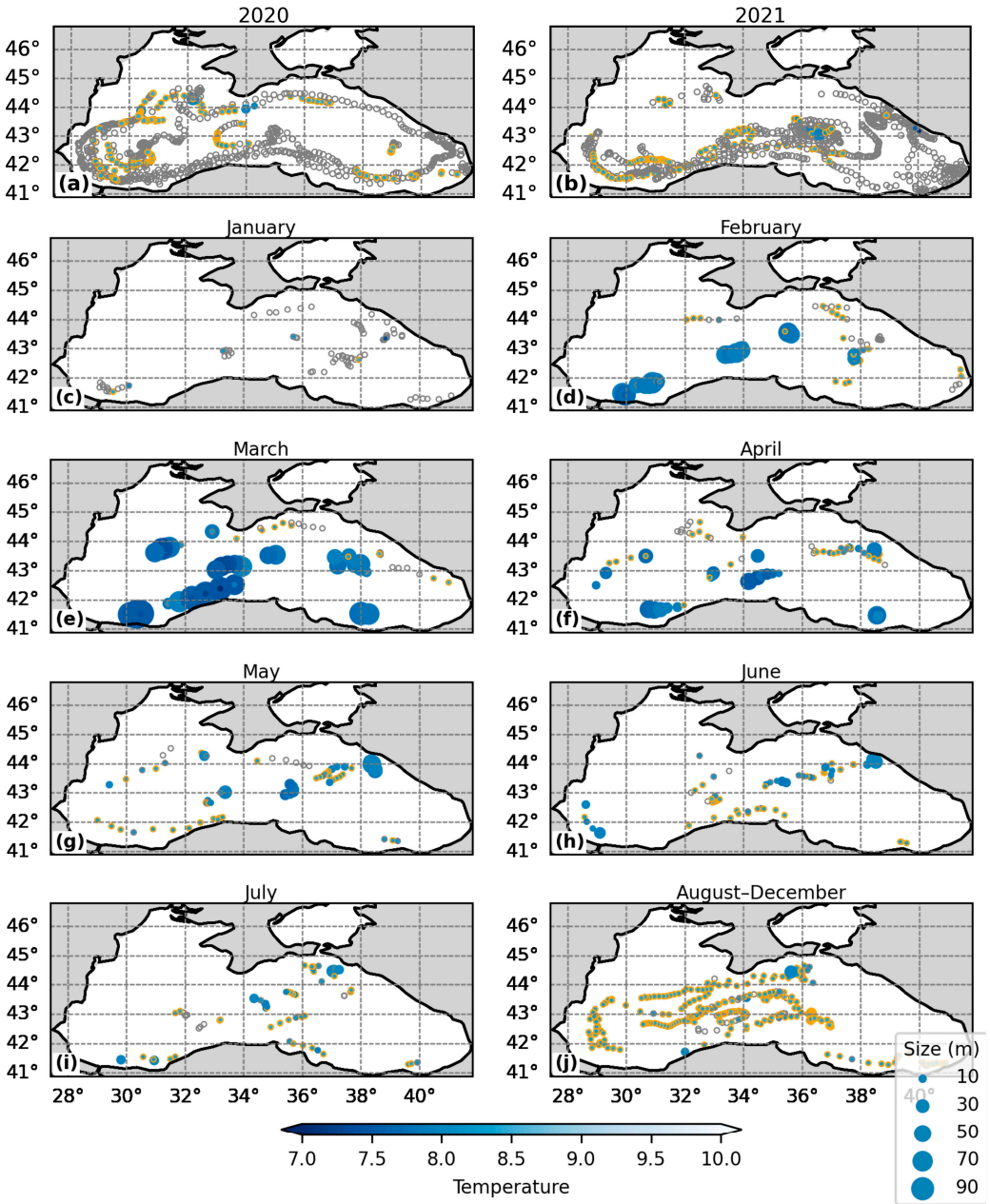

Figure 7. Argo float measurements: means of temperatures below 8 °C are shown by blue circles that darken with lower temperatures; the size of the circles indicates the thickness of the cold layer below 8 °C, while the temperatures of the water column, between 8 °C and 8.5 °C, are indicated with orange circles, without any thickness information being provided. Finally, gray circles show that none of the two temperature-related conditions were met in the position of the float profile. Whole-year compositions are shown in (**a**) for 2020 and in (**b**) for 2021 and 2022; monthly compositions are indicated for (**c**) January, (**d**) February, (**e**) March, (**f**) April, (**g**) May, (**h**) June, (**i**) July, and (**j**) August to December.

Thicknesses of the CIL were lower in the cyclonic interior region compared to the periphery region because pronounced upwelling caused the denser deep isopycnal surfaces to become shallower (Figures 4j,k and 5a). On the other hand, anticyclones, having weaker

stability, allowed deeper ventilation, leading to thicker CIL formation. In March 2022, the deepest CIL formation was observed in the Sakarya anticyclone, close to the Bosphorus, with a depth of 100 m; in addition, several others were reported, with ~70 m along the Anatolian periphery and the NWS continental slope.

As the seasonal warming process began in April, a thermocline emerged in the upper 25–30 m. Therefore, the cold-water mass was squeezed between the seasonal thermocline and the permanent pycnocline (Figure 7f). In May, the CIL observations persisted primarily in the cyclonic interior while the CIL temperatures rose slightly. The temperatures of the CIL along the western periphery exceeded 8 °C, except for the few thin-CIL observations (less than 10 m). While CIL formation was not observed on the Rim Current periphery from the Caucasus to the Crimea costal area in March, it appeared in April and persisted between May and June in the Caucasus periphery. The CIL observations later in summer suggested CIL formation based on advection along the Rim Current and its periphery. The advective CIL formations are frequently mentioned in previous studies [12,15,33]. Examining the months after April, random distribution of the CIL can be attributed to isopycnal spreading inside the cyclonic interior due to mesoscale processes inside the cyclonic interior [9,12]. The temperatures continued to rise during the summer, with most of the float recording CIW temperatures exceeding 8 °C (Figure 7g–j). Warming of the CIL was slower in the western cyclonic and coastal areas compared to the eastern part of a region; nevertheless, temperatures of the CIL increased gradually by ~0.5 °C until the end of the year.

It is worth noting that the western periphery area was rarely observed by Argo floats in 2022. The irregular thickness of the CIL between spring and summer was most probably related to the distance of the float from the anticyclonic eddy structures along the periphery of this region. CIL formation was observed only after April in the Caucasus and Kerch anticyclonic area. CIL observations in this region from late spring suggest isopycnal spreading, likely driven by advection from the Rim Current or onshore excursions from the eastern basin influenced by mesoscale features.

Using the warm CIL criterion (<8.35 °C) proposed by Capet et al. [5] (shown in the Supplementary Materials, Figure S2), only a few more weak cold-water formations were detected in the northwestern continental slope and cyclonic gyres during the winters of 2020 and 2021, with no detections occurring in the rest of the year.

Figure 8 shows the T-S distributions for the autumn months of the years 2020, 2021, and 2022. The slope of the T-S distribution curve at the base of the CIL (between σ_t = 16 and σ_t = 16.75) decreased from 2020 to 2021. A dramatic drop in the steepness of the T-S curve at the bottom of the CIL occurred in 2022. The curvature in the core of the T-S graphic increased, the mixing curve became non-linear, and the steepness of the mixing curve at σ_t = 15.5 changed substantially, indicating intensified diapycnal mixing at this depth.

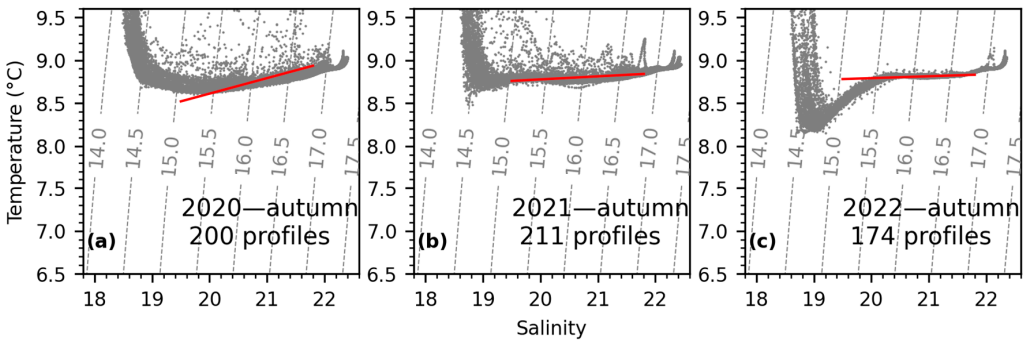

Figure 8. Autumn distribution of T-S for the years (**a**) 2020, (**b**) 2021, and (**c**) 2022. These lines are the linear regression lines of the distribution between σ_t = 16 and σ_t = 16.75. Multiple cycles of the float for the same day are represented by one full profile of the float.

The changes in CIL structure in autumn seasons (distant from the period of winter convection) between 2005 and 2019 were studied by Stanev, E.V., and Chtirkova, B. [18]. They compared the slopes of the T-S distribution curves at the base of the CIL and showed a dramatic change in the slope in 2012. The study concluded that the slopes of the T-S curves below the core of the CIL decreased over the period that they analyzed, suggesting a diminished influence of temperature in these layers of the water column. The flattening trend in the slopes of the T-S curves at the same levels continued for the years 2020, 2021, and 2022, as shown in this study. The substantial change that occurred in 2021 persisted with intense mixing conditions in 2022 (Figure 8). The distributions for the entire year are provided in the Supplementary Materials (Figure S3).

5. Discussion

In mid-March 2022, the Siberian High, associated with intense cold-air masses, caused severe weather conditions across southern Europe, including the Black Sea. These anomalies resulted in exceptionally low atmospheric and sea-water temperatures, with the average air temperature dropping to 0 °C and CIW temperatures reaching 7.3 °C. The winters of 2020 and 2021 were unusually warm: the highest mean winter SST (10 °C) since the 1960s was recorded. Following these successive warm winters, the cold episodes of March 2022 triggered convective mixing, which entrained water masses that lacked a remnant CIL from previous years, leading to more pronounced convective mixing observed in Argo float recordings.

This event provided a unique opportunity to observe widespread CIW generation across extensive areas, including the cyclonic interior, the Rim Current, and its periphery, except for the northeastern periphery. These findings contribute to a better understanding of CIL dynamics, particularly under extreme conditions in the Black Sea.

There is a growing consensus regarding CIL formation in the Black Sea. The most widely accepted explanations include (1) convection occurring in the centers of cyclonic gyres during winter and (2) horizontal transport of cold-water masses from the NWS carried by the Rim Current and eddy formations along the shelf break [12–15,33]. During the warm winters preceding 2022, CIW formation was rare and mostly confined to the northwestern continental slope and cyclonic gyres. This observational evidence reinforces the understanding that the main cyclonic gyres and the NWS continental slope are critical areas for CIL formation.

The evaluation of CIW formation during the cold invasion in the Black Sea has not been observationally documented in the spatial and temporal domains previously. Therefore, this study provides observational evidence of widespread convective formation of CIW because of the intense cold episodes in March 2022. The distribution of SSTs and SSTAs showed an increase from west to east. The thickness and cold-water content of the CIW decreased in accordance with the preconditioning phase.

The intensification of the Rim Current resulted in strong upwelling of relatively dense deep waters within the cyclonic interior region. Convective mixing over the dome-shaped pycnocline allowed cold surface water to penetrate deeper isopycnic levels, making the upper water column above the pycnocline colder and saltier. The deeper pycnocline in the western cyclonic gyre enabled deeper penetration of winter cooling, resulting in thicker CIL formations in the west, compared to the east, in the cyclonic interior basin. Under these conditions, the CIL formations in the eastern part of the cyclonic interior were warmer and thinner than those in the west.

Anticyclonic eddies along the northwestern and southern periphery of the Rim Current had thicker CIL formations. The results of this study are consistent with previous findings, indicating that the weaker stability of the surface layer above the pycnocline in these anticyclonic eddies facilitated deeper ventilation [12,16]. Although cooling in the water column was also effective in the northeastern anticyclonic coastal area, the relatively warm waters of the region, as well as the warm waters advected by local dynamics, hindered convection during the cold episodes. However, after the cooling period, in late spring and

summer, the local dynamics—driven by eddy motion, Rim Current meanders, and offshore filaments—spread the CIW mass over the region.

CIL observations distant from the winter convection period in the northeastern basin and the persistence of the CIL throughout the summer in the eastern cyclonic area support the model results of Stanev et al. (2003) [14], which suggest that CIL formations in this region are primarily due to the transport of cold-water masses into this part of the basin. However, unlike these authors, observations in the southeastern periphery region in 2022 indicate that convective CIL formation is comparable to advective formation.

The studies by Stanev and Chtirkova (2021) [18] and Stanev et al. (2019) [20], based on Argo float data collected between 2005 and 2019, highlight a warming trend and the potential disappearance of the CIL. Hence, the results of this study demonstrate that the trends identified in those studies continued and even intensified in 2020 and 2021. The further reduction in T-S curve slopes (Figure 8b,c) at the base (between σ_t = 16 and σ_t = 16.75) of the CIL in 2021 and 2022 emphasizes the ongoing trend of the decreasing role of temperature on stratification in the Black Sea.

6. Conclusions

This study provides valuable insights into the formation and spread of cold intermediate water (CIW) in the Black Sea, particularly during the anomalously cold events of March 2022. Utilizing data from Argo floats, Copernicus CMEMS, and ERA5, the research demonstrates how cold air masses from the Siberian High drastically impacted the Black Sea's thermal structure. The sharp drop in air and sea temperatures during these cold episodes created favorable conditions for convective mixing, leading to widespread CIW formation across the region.

The remnants of the cold intermediate layer (CIL) from the warm winters of 2020 and 2021 provided a unique opportunity to observe how newly formed CIW spread after the convective mixing of 2022. This study offers an evidence-based evaluation of CIW formation and distribution in the Black Sea. The findings revealed extensive CIW formation in both the cyclonic interior and peripheral regions, excluding the northeastern periphery, supporting existing theories of CIW formation, including the role of convection within cyclonic gyres and cold-water advection from the Northwestern Shelf.

Notably, during the cold episodes of March 2022, a significant geographical gradient in CIW characteristics was observed, marked by an increase in temperatures from west to east, consistent with the distribution of sea surface temperatures. Concurrently, the sizes of CIW were larger in the western cyclonic gyre compared to the eastern one. Furthermore, the cold waters produced during these episodes, spread isopycnally throughout the summer months, eventually reaching northeastern and eastern regions where no CIW mass formation occurred during the winter.

Additionally, this study corroborated the warming trends noted in previous research, confirming that this warming has continued—and intensified—over recent years. The reduction in the slope of the temperature–salinity (T-S) curve at the CIL base further suggests a diminishing role of temperature in the stratification processes within the Black Sea.

Supplementary Materials: The following supporting information can be downloaded at: https://www.mdpi.com/article/10.3390/jmse12112027/s1, Figure S1. Tracks of 12 ARGO floats analyzed between February and May 2022; Figure S2. Float measurements; Figure S3. Distribution of T-S for the years 2020, 2021, and 2022; Figure S4. Surface monthly mean SST values for 2020 (a–d) and 2021 (e–h) for January to April were obtained from the Copernicus CMEMS gridded SST product.

Funding: This research received no external funding.

Institutional Review Board Statement: Not applicable.

Informed Consent Statement: Not applicable.

Data Availability Statement: The data used in the study are available at https://data.marine.copernicus.eu/product/SST_BS_SST_L4_REP_OBSERVATIONS_010_022/description and https://data.marine.copernicus.eu/product/SEALEVEL_EUR_PHY_L4_MY_008_068/description, accessed on 2 June 2023. The ECMWF data used in this study were obtained from https://cds.climate.copernicus.eu/datasets/reanalysis-era5-single-levels?tab=overview, accessed on 2 October 2024. The Argo data were collected and made freely available by the International Argo Program and the national programs that contribute to it (https://argo.ucsd.edu, https://www.ocean-ops.org). The Argo Program is part of the Global Ocean Observing System.

Acknowledgments: The author thanks Sinan Şahinoğlu for sharing his experience with ECMWF data and thanks Sancan Çokacar for language support. The author also extends sincere gratitude to the reviewers for their valuable comments and constructive suggestions, which have significantly enhanced the quality of this manuscript. Argo data were collected and made freely available by the International Argo Program and the national programs that contribute to it (https://argo.ucsd.edu, https://www.ocean-ops.org). The Argo Program is part of the Global Ocean Observing System. The data presented in this study are available on request from the author.

Conflicts of Interest: The author declares that they have no known competing financial interests or personal relationships that could have appeared to influence the work reported in this paper.

Declaration of Generative AI: The author used ChatGPT 3.5, available at https://chat.openai.com/, in order to enhance the readability and writing style. After using this tool/service, the author reviewed and edited the content as needed and takes full responsibility for the content of the publication.

References

1. Capet, A.; Barth, A.; Beckers, J.-M.; Marilaure, G. Interannual variability of Black Sea's hydrodynamics and connection to atmospheric patterns. *Deep Sea Res. Part II Top. Stud. Oceanogr.* **2012**, *77–80*, 128–142. [CrossRef]
2. Cherneva, Z.; Andreeva, N.; Pilar, P.; Valchev, N.; Petrova, P.; Guedes Soares, C. Validation of the WAMC4 wave model for the Black Sea. *Coast. Eng.* **2008**, *55*, 881–893. [CrossRef]
3. Efimov, V.V.; Komarovskaya, O.I. Spatial Structure and Recurrence of Large-Scale Temperature Anomalies of the Sea Surface Temperature in the Black Sea. *Oceanology* **2018**, *58*, 155–163. [CrossRef]
4. Özsoy, E.; Ünlüata, Ü. Oceanography of the Black Sea: A review of some recent results. *Earth-Sci. Rev.* **1997**, *42*, 231–272. [CrossRef]
5. Capet, A.; Vandenbulcke, L.; Grégoire, M. A new intermittent regime of convective ventilation threatens the Black Sea oxygenation status. *Biogeosciences* **2020**, *17*, 6507–6525. [CrossRef]
6. Efimov, V.V.; Yarovaya, D.A. Numerical simulation of air convection in the atmosphere during the invasion of cold air over the Black Sea. *Izv. Atmos. Ocean. Phys.* **2014**, *50*, 610–620. [CrossRef]
7. Kubryakov, A.A.; Belokopytov, V.N.; Zatsepin, A.G.; Stanichny, S.V.; Piotukh, V.B. The Black Sea Mixed Layer Depth Variability and Its Relation to the Basin Dynamics and Atmospheric Forcing. *Phys. Oceanogr.* **2019**, *26*, 397–413. [CrossRef]
8. Oguz, T.; Latun, V.S.; Latif, M.A.; Vladimirov, V.V.; Sur, H.I.; Markov, A.A.; Özsoy, E.; Kotovshchikov, B.B.; Eremeev, V.V.; Ünlüata, Ü. Circulation in the surface and intermediate layers of the Black Sea. *Deep. Sea Res. Part I Oceanogr. Res. Pap.* **1993**, *40*, 1597–1612. [CrossRef]
9. Oguz, T.; Besiktepe, S. Observations on the Rim Current structure, CIW formation and transport in the western Black Sea. *Deep. Sea Res. Part I Oceanogr. Res. Pap.* **1999**, *46*, 1733–1753. [CrossRef]
10. Korotaev, G. Seasonal, interannual, and mesoscale variability of the Black Sea upper layer circulation derived from altimeter data. *J. Geophys. Res.* **2003**, *108*, 3122. [CrossRef]
11. Sur, H.İ.; Özsoy, E.; Ünlüata, Ü. Boundary current instabilities, upwelling, shelf mixing and eutrophication processes in the Black Sea. *Prog. Oceanogr.* **1994**, *33*, 249–302. [CrossRef]
12. Ivanov, L.I.; Backhaus, J.O.; Özsoy, E.; Wehde, H. Convection in the Black Sea during cold winters. *J. Mar. Syst.* **2001**, *31*, 65–76. [CrossRef]
13. Shapiro, G.I.; Wobus, F.; Aleynik, D.L. Seasonal and inter-annual temperature variability in the bottom waters over the western Black Sea shelf. *Ocean Sci.* **2011**, *7*, 585–596. [CrossRef]
14. Stanev, E.V.; Bowman, M.J.; Peneva, E.L.; Staneva, J.V. Control of Black Sea intermediate water mass formation by dynamics and topography: Comparison of numerical simulations, surveys and satellite data. *J. Mar. Res.* **2003**, *61*, 59–99. [CrossRef]
15. Miladinova, S.; Stips, A.; Garcia-Gorriz, E.; Macias Moy, D. Formation and changes of the Black Sea cold intermediate layer. *Prog. Oceanogr.* **2018**, *167*, 11–23. [CrossRef]
16. Akpinar, A.; Fach, B.A.; Oguz, T. Observing the subsurface thermal signature of the Black Sea cold intermediate layer with Argo profiling floats. *Deep Sea Res. Part I Oceanogr. Res. Pap.* **2017**, *124*, 140–152. [CrossRef]

17. Kubryakova, E.A.; Kubryakov, A.A.; Stanichny, S.V. Impact of Winter Cooling on Water Vertical Entrainment and Intensity of Phytoplankton Bloom in the Black Sea. *Morskoy Gidrofiz. Zhurnal* **2018**, *25*, 206–222. [CrossRef]
18. Stanev, E.V.; Chtirkova, B. Interannual Change in Mode Waters: Case of the Black Sea. *J. Geophys. Res. Ocean.* **2021**, *126*, e2020JC016429. [CrossRef]
19. Miladinova, S.; Stips, A.; Garcia-Gorriz, E.; Macias Moy, D. Black Sea thermohaline properties: Long-term trends and variations. *J. Geophys. Res. Ocean.* **2017**, *122*, 5624–5644. [CrossRef]
20. Stanev, E.V.; Peneva, E.; Chtirkova, B. Climate Change and Regional Ocean Water Mass Disappearance: Case of the Black Sea. *J. Geophys. Res. Ocean.* **2019**, *124*, 4803–4819. [CrossRef]
21. Capet, A.; Stanev, E.V.; Beckers, J.-M.; Murray, J.W.; Grégoire, M. Decline of the Black Sea oxygen inventory. *Biogeosciences* **2016**, *13*, 1287–1297. [CrossRef]
22. Staneva, J.V.; Stanev, E.V. Water mass formation in the Black Sea during 1991–1995. *J. Mar. Syst.* **2002**, *32*, 199–218. [CrossRef]
23. Cokacar, T.; Kubilay, N.; Oguz, T. Structure of Emiliania huxleyi blooms in the Black Sea surface waters as detected by Sea WIFS imagery. *Geophys. Res. Lett.* **2001**, *28*, 4607–4610. [CrossRef]
24. Oguz, T.; Cokacar, T.; Malanotte-Rizzoli, P.; Ducklow, H.W. Climatic warming and accompanying changes in the ecological regime of the Black Sea during 1990s. *Glob. Biogeochem. Cycles* **2003**, *17*. [CrossRef]
25. Oguz, T.; Dippner, J.W.; Kaymaz, Z. Climatic regulation of the Black Sea hydro-meteorological and ecological properties at interannual-to-decadal time scales. *J. Mar. Syst.* **2006**, *60*, 235–254. [CrossRef]
26. Merchant, C.J.; Embury, O.; Bulgin, C.E.; Block, T.; Corlett, G.K.; Fiedler, E.; Good, S.A.; Mittaz, J.; Rayner, N.A.; Berry, D.; et al. Satellite-based time-series of sea-surface temperature since 1981 for climate applications. *Sci. Data* **2019**, *6*, 223. [CrossRef]
27. Pisano, A.; Buongiorno Nardelli, B.; Tronconi, C.; Santoleri, R. The new Mediterranean optimally interpolated pathfinder AVHRR SST Dataset (1982–2012). *Remote Sens. Environ.* **2016**, *176*, 107–116. [CrossRef]
28. Argo. Argo Float Data and Metadata from Global Data Assembly Centre (Argo GDAC). 2000. Available online: https://www.seanoe.org/data/00311/42182/ (accessed on 2 June 2023).
29. Wong, A.P.S.; Wijffels, S.E.; Riser, S.C.; Pouliquen, S.; Hosoda, S.; Roemmich, D.; Gilson, J.; Johnson, G.C.; Martini, K.; Murphy, D.J.; et al. Argo Data 1999–2019: Two Million Temperature-Salinity Profiles and Subsurface Velocity Observations From a Global Array of Profiling Floats. *Front. Mar. Sci.* **2020**, *7*, 568494. [CrossRef]
30. Belkin, I.M. Rapid warming of Large Marine Ecosystems. *Prog. Oceanogr.* **2009**, *81*, 207–213. [CrossRef]
31. Ginzburg, A.I.; Kostianoy, A.G.; Sheremet, N.A. Sea Surface Temperature Variability. In *The Black Sea Environment*; Springer: Berlin/Heidelberg, Germany, 2007; pp. 255–275.
32. Çokacar, T. Spatial and Temporal Variability of the Surface Temperature in the Black Sea Between 2000-2022. *Çanakkale Onsekiz Mart Univ. J. Mar. Sci. Fish.* **2023**, *6*, 158–165. [CrossRef]
33. Stanev, E.V.; He, Y.; Staneva, J.; Yakushev, E. Mixing in the Black Sea detected from the temporal and spatial variability of oxygen and sulfide—Argo float observations and numerical modelling. *Biogeosciences* **2014**, *11*, 5707–5732. [CrossRef]